Nonlinear Aerodynamic Effects on Bodies in Supersonic Flow

James L. Pittman*
NASA Langley Research Center, Hampton, Virginia
and
Michael J Sicari†
Grumman Aerospace Corporation, Bethpage, New York

The supersonic flow about generic bodies was analyzed to identify the elements of the nonlinear flow and to determine the influence of geometry and flow conditions on the magnitude of these nonlinearities. The nonlinear effects were attributed to separated-flow and attached-flow nonlinearities. The nonlinear attached-flow contribution was further divided into large-disturbance effects and entropy effects. Conical, attached-flow boundaries were developed to illustrate the flow regimes where the nonlinear effects are significant, and the use of these boundaries for angle of attack and three-dimensional geometries was indicated. Normal-force and pressure comparisons showed that the large-disturbance and separated-flow effects were the dominant nonlinear effects at low supersonic Mach numbers and that the entropy effects were dominant for high supersonic Mach number flow. Both cross-sectional shape and longitudinal geometry variations influenced significantly the development of the nonlinear effects. The magnitude of all the nonlinear effects increased with increasing angle of attack. A full-potential method, NCOREL, which includes an approximate entropy correction, was shown to provide accurate attached-flow pressure estimates from Mach 1.6 through 4.6.

Nomenclature

$C_{D_{wave}}$ = volumetric wave drag at $\alpha = 0$ deg
C_N = normal force coefficient, $\dfrac{\text{Normal force}}{q_\infty S}$
C_p = pressure coefficient, $\dfrac{p - p_\infty}{q_\infty}$
L = body length
M = freestream Mach number
p = local body surface pressure
p_∞ = freestream static pressure
q_∞ = freestream dynamic pressure
S = reference area
X = axial coordinate from body nose
α = angle of attack, deg
δ = cone semivertex angle, deg
θ = polar coordinate angle, deg

Introduction

ACCURATE design and analysis of flight vehicles requires a detailed understanding of the aerodynamics of arbitrary shapes. The supersonic flow about missile configurations is of particular interest, though many of the lessons drawn from missile configurations are equally applicable to aircraft forebody problems. A great deal of effort has been devoted to the development of supersonic missile aerodynamic prediction methods, especially for the high angle-of-attack flow situation where the leeside flow is generally separated from the body surface and a system of vortices is formed. These predictive codes for missile configurations can generally be characterized as data base methods[1] or linear-theory methods, which include techniques for calculating separated-flow effects.[2] These methods tend to provide reasonable first-order estimates of integrated forces and moments within a limited range of geometries and Mach numbers, though the local surface pressures are often inaccurate. Studies of supersonic missile configurations with noncircular-body cross sections, developed for improved cruise performance or for weapons carriage, revealed deficiencies in the state-of-the-art missile aerodynamic predictive methods. These deficiencies led to a detailed study of the flowfield about an elliptic missile body at a Mach number of 2.5. (Ref. 3). This study showed that the nonlinear effects due to both attached flows and separated flows contributed significantly to the local surface pressures and to the overall forces and moments. These results served as the impetus for the present, more general investigation of the supersonic flow about generic body shapes.

This paper presents the results of a study conducted in order to identify the nonlinear flow features on bodies of circular and elliptic cross section in supersonic flow, and to accurately determine the magnitude of these nonlinear effects across a wide Mach number and angle-of-attack range. Both two-dimensional (conical) and three-dimensional (nonconical) bodies were studied across the Mach number range from 1.6 to 4.6 through angles of attack as high as 28 deg. The nonlinear flow is broken down into attached-flow and separated-flow effects. The nonlinear attached-flow is directly calculated by an inviscid method and the results are discussed in detail in this report. The magnitude of the separated-flow nonlinear effects is indirectly estimated because sufficiently accurate direct prediction methods are not presently available.

General Approach

The nonlinear-flow effects are defined as those effects which are not calculated by the linear-potential theory. These nonlinear-flow effects are defined as attached, nonlinear-flow effects and separated, nonlinear-flow effects. The attached, nonlinear-flow effects are further divided into large-disturbance effects and entropy effects.

Presented as Paper 84-0231 at the AIAA 22nd Aerospace Sciences Meeting, Reno, Nev., Jan. 9-12, 1984; received Feb. 7 1984; revision received May 16, 1984. This paper is declared a work of the U.S. Government and therefore is in the public domain.

*Aero-Space Technologist, Supersonic Aerodynamics Branch, High-Speed Aerodynamics Division. Member AIAA.

†Staff Scientist, Grumman Research and Development Center. Member AIAA.

A simple guideline for analyzing the attached flowfield is presented in Fig 1 This figure was developed by considering the supersonic flow over a circular cone at $\alpha = 0$ deg Four distinct flow regions are shown on this boundary chart The transonic flow boundary is for a sonic surface Mach number which can be determined from cone tables [4] The boundary between the linear theory and large-disturbance regions is defined as the point where the difference between the surface pressure computed by linear theory[5,6] and the surface pressure computed by full potential theory[7] is 10% Similarly, the boundary between the large disturbance and entropy regions represents a 10% difference between the surface pressure computed by the full potential theory and the exact, inviscid cone solution [4] For reference, the curve for the hypersonic similarity parameter of value unity ($M\delta = 1$) is also shown on the figure

The information in Fig. 1 shows that the region of accurate linear theory pressure estimates is quite small and that the full-potential method, which includes the large disturbance effect, has a much greater range of applicability than the linear theory Entropy effects do not seem to be significant for $M < 2$, at least for attached flow Conditions at angle of attack can be analyzed by considering the sum of the cone angle and the angle of attack This conical attached flow boundary chart can also be applied to three-dimensional bodies by using a nonconical method developed by Mason [8]

In the present paper, the nonlinear effects are studied by concentrating on the surface-pressure coefficients for local effects and on the normal force coefficients for integrated effects Pressure-coefficient and normal force "increments" are used throughout this study to quantify the magnitude of the nonlinear effects An illustration of these increments is presented in Fig 2 The large-disturbance increment is defined as the difference between a linear theory solution[5,6] and the nonlinear, full-potential solution,[7] whereas the en tropy increment, which represents the losses in the inviscid flow field, is the difference betwen the nonlinear, full-potential solution and an Euler solution. Both of these attached-flow increments are shown in Fig 2 on the normal-force and pressure-coefficient plots. The large-disturbance increment yields an increase in the normal force and, generally, an increase in the magnitude of the pressure coefficient relative to the linear theory The effect of entropy (indicated on Fig 2 by the downward pointing arrow) is to decrease both the normal force and the pressure coefficient The pressure-coefficient plot shows that the entropy increment is almost totally confined to the lower surface, though entropy can affect the leeward surface when the leeward surface flow is attached

The nonlinear separated-flow normal force increment is defined as the difference between the experiment and the sum of 1) an Euler solution for the lower surface, and 2) a linear-theory solution for the upper surface The lower surface and the upper surface are arbitrarily divided at $\theta = 90$ deg, which effectively forces the flow separation point to that location This indirect procedure for determining the separated-flow increment is employed because sufficiently accurate methods for calculating the separated flow are not available As a result of this procedure, the separated-flow increment is calculated for normal force only Although the subject is not discussed in detail in this paper, the pressure coefficient plots can be used to determine the angle of attack and the surface location at which separation occurs by observing the full-potential and experimental pressure coefficient distribution in the vicinity of the leading edge The surface location at which the full potential pressure coefficient departs from the ex perimental data has been shown previously to correlate with the beginning of a separated flow region.[3]

It is important to emphasize that the normal force comparisons do not represent a straightforward data theory comparison for those cases where separated flow exists This is a consequence of the present procedure for quantifying the

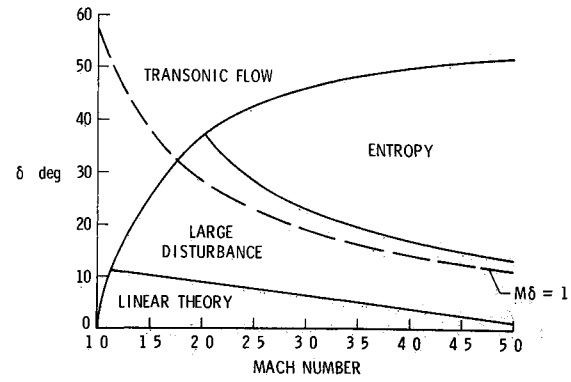

Fig 1 Attached flow boundary chart for a circular cone at $\alpha = 0$ deg

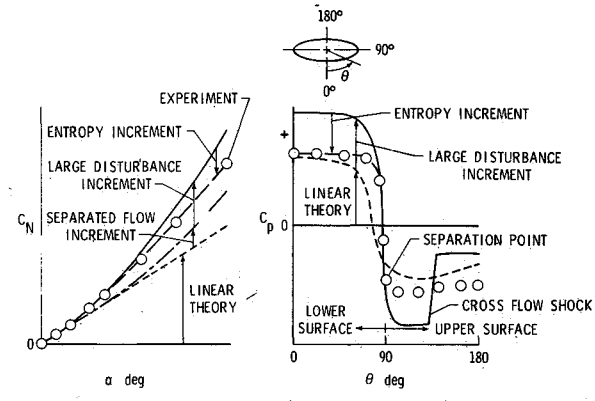

Fig. 2 Typical nonlinear flow increments at high angle of attack.

nonlinear increments which relies on both calculated and experimental data Specifically, a simple summation of the nonlinear attached flow increments with the linear-theory solution does not provide the total nonlinear attached flow solution because the nonlinear attached flow increment is meaningless in the separated flow region, and therefore, is replaced with an experimentally derived separated-flow increment

A new method for the calculation of an approximate entropy correction has been developed by Siclari[9] and incorporated into the full potential (NCOREL) code [7] This approximate entropy calculation is obtained with little additional computational effort and suffers no significant loss in accuracy compared with a full Euler solution for an attached flow The accuracy of this procedure was demonstrated in Ref. 9 for conical geometries. Consequently, the entropy increments presented in this paper are differences between full-potential (NCOREL) solution results obtained with and without the approximate entropy correction This procedure for obtaining the entropy increment ensures that it is not a function of grid size, convergence criteria, integration techniques, etc ,—a situation which might occur if two different codes were used to calculate this increment

Normal-Force Analysis

In this section the effects of geometry and flow conditions on the nonlinearities are presented in terms of normal-force increments and representative surface pressure distributions First, the effects of different body cross-section geometries are examined using unpublished NASA force data and pressure data[10] taken at $X/L = 0\ 25$ for a circular cone and a 3:1 elliptic cross section cone of equivalent planform The effects of longitudinal geometry variations are then presented using normal force and pressure data for a circular arc cylinder of circular cross section[11,12] and for an Adams' minimum drag body of 3:1 elliptic cross section [13,14]

Effect of Cross Section Geometry

The first case considered is the 20 deg circular cone at $M=1\ 70$ The experimental data presented in Fig 3 go through a maximum 21 deg angle of attack which corresponds to 41 deg of flow deflection on the lower surface centerline The normal force comparison shows that the linear theory solution is perhaps more accurate than one would expect for this severe flow deflection angle, but a significant con tribution to the normal force from both the large disturbance increment and the entropy increment is noted at the higher angles of attack The large-disturbance increment is apparent at $\alpha \approx 2$ deg, but the entropy increment does not produce an effect until $\alpha \approx 10$ deg The magnitude of both of these nonlinear increments increases with increasing angle of at tack As mentioned previously, the entropy increment decreases the normal-force estimate The surface pressure data for the circular cone at $\alpha=21\ 01$ deg are also shown in Fig 3. Note the rapid decrease in pressure on the lower surface as θ increases The large disturbance increment is nearly uniform around the circumference of the body except for a small region in the upper surface The entropy increment is, in general, small and confined to the lower surface with the largest effect being on the lower-surface centerline This occurs because the entropy is a function of the bow shock strength, which is strongest at the lower surface centerline and decreases away from that point The agreement between the upper surface experimental pressure and the predicted at tached flow pressure does not indicate the presence of flow separation

Normal force and pressure-coefficient comparisons for the elliptic cone at $M=1\ 70$ are shown in Fig 4. The most significant difference between the circular cone and the elliptic cone is the presence of a separated flow region on the

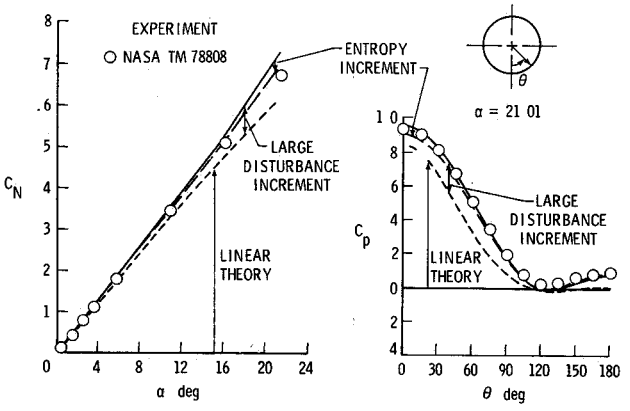

Fig 3 Normal force and pressure coefficient comparisons for the 20 deg circular cone at $M_\infty = 1\ 70$

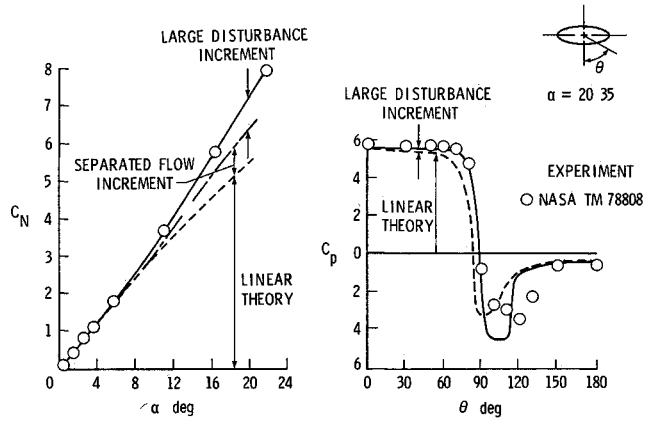

Fig 4 Normal force and pressure coefficient comparisons for the 3:1 elliptic cone at $M_\infty = 1\ 70$

leeward surface of the elliptic cone The large disturbance effect produces a significant positive normal force increment which is roughly the same magnitude as the separated flow increment Also, the large disturbance increment for the elliptic cone is approximately the same magnitude as that of the circular cone There is no significant normal force entropy increment for the flow about the elliptic cone at $M=1\ 70$ because of the reduced flow deflection angles on the lower surface The distribution of the pressure coefficient data on the elliptic cone at $\alpha=20\ 35$ deg shows a much different character than was observed for the circular cone at high angle of attack The pressure distribution across the lower surface is nearly constant followed by a rapid expansion around the leading edge ($\theta=90$ deg) onto the upper surface In contrast to the nearly constant large disturbance increment that was noted in the pressure distribution for the 20 deg circular cone, the large-disturbance increment for the elliptic cone varies significantly around the body The large discrepancy in pressures between the full potential method and the experimental data, which is observed at high angles of attack on the upper surface slightly inboard of the leading edge ($\theta>90$ deg), indicates the presence of flow separation The full-potential code predicts an attached flow pressure distribution which is characterized by an expansion peak near the leading edge ($\theta=90$ deg) followed by a strong crossflow shock Although it is obvious from the experimental data that the real flow separates, it is interesting to note that the at tached flow pressures result in compensating errors Because of these compensating errors, the fully attached flow normal force calculated by the full potential method is in remarkably good agreement with the experimentally measured normal force (see Ref 3)

The effect of increasing Mach number is illustrated in Fig 5 where the normal force and a circumferential pressure distribution are analyzed for the circular cone at $M=2\ 50$ Compared with the $M=1\ 7$ results, the increased magnitude of both the large disturbance increment and the entropy increment is readily apparent; in fact, at $M=2\ 50$, the entropy increment becomes noticeable at $\alpha \approx 1$ deg whereas at $M=1\ 7$ the entropy increment appeared at $\alpha \approx 10$ deg In addition to decreasing the normal force estimate, the entropy increment also linearizes the normal force vs α curve The pressure comparison at $\alpha=20\ 95$ deg substantiates the trends indicated in the analysis of the normal-force data In particular, note the magnitude of the entropy effect on the lower surface

The normal force variation and a typical pressure distribution are shown in Fig 6 for the elliptic cone at $M=2\ 50$ The normal force analysis shows that all three nonlinear effects are present in this instance, and that the magnitude of each nonlinear increment increases with in creasing angle of attack Near the upper end of the angle of attack range, the entropy increment nearly cancels the large disturbance increment The pressure variation around the body at $\alpha=20\ 49$ deg is presented on the right hand side of the figure Over most of the lower surface the linear theory overestimates the compression pressures, which is an unusual occurrence possibly related to the proximity of the body to the freestream Mach cone; however, the large disturbance in crement is still in the proper direction to improve the agreement between theory and experiment The full potential theory overestimates the compression pressure, whereas the entropy correction seems to slightly overcorrect in this in stance The separated flow region is evident on the upper surface

At $M=4\ 50$, a linear theory solution based on a surface distribution of source panels is not available for either the circular or the elliptic cone because the freestream Mach cone lies inside the body Consequently, neither the large disturbance increment nor the vortex increment can be determined The theory presented for the 20 deg circular cone at $M=4\ 50$ in Fig 7 is the full potential theory (NCOREL) with and without the entropy correction It is apparent from

the data comparison that the entropy effects are significant at high Mach number. In fact, without the entropy correction a full-potential solution could overpredict the normal force by a factor of two at higher Mach numbers. The excellent agreement between attached-flow and experimental normal force and pressures indicates no significant effect of flow separation on the circular cone. Figure 8 contains the $M=4.50$ data for the 3:1 elliptic cone. The effect of entropy is slightly reduced compared to the circular cone case, but it is still very significant, as is shown for both the normal-force and the pressure-coefficient curves. The pressure variation at $\alpha=19.50$ deg indicates the significance of the entropy increment, the accuracy of the approximate entropy correction, and the fact that the entropy effect is almost entirely confined to the lower surface. Also note that the entropy increment is nearly constant on the lower surface. On the upper surface ($\theta>90$ deg), it appears that there is a separated-flow region evidenced by the disparity between the full-potential theory and the experimental data. Although flow separation still occurs at high Mach number, its effect on the local pressure coefficient and on the integrated forces and moments tends to diminish because the expansion pressures cannot exceed the vacuum limit which is a function of M^{-2}

Effect of Longitudinal Geometry

The effect of longitudinal geometry changes on the flow nonlinearities is illustrated by comparing results for three-dimensional bodies with those previously discussed for two-dimensional bodies of similar cross section. For bodies with circular cross sections, results for a circular-arc cylinder[11,12] are presented and compared with those for a circular cone and, for bodies with elliptic cross sections, results for an Adams' minimum drag body of 3:1 elliptic cross section[13,14] are presented and compared with those for the 3:1 elliptic cross-section cone.

Normal-force results for $M=1.60$, 2.96, and 4.63 are presented in Fig. 9 for the circular-arc cylinder of circular cross section. The circular cone was analyzed at approximately the same Mach numbers to help define the effects of longitudinal geometry variations on the nonlinear-flow increments. The most significant difference relating to longitudinal geometry variations is that the separated-flow increment on the circular-arc cylinder is a large contributor to the normal force at $M=1.60$ and 2.96. By contrast, the circular cone did not show any separation effects. Also, the contribution to the normal force from the large-disturbance increment is much larger on the circular-arc cylinder than was noted on the circular cone. Both the separated-flow and the large-disturbance increments decrease in magnitude with increasing Mach number. Entropy does not significantly affect the flow at $M=1.60$ but does produce an appreciable contribution to the normal force at $M=2.96$ and 4.63. Although the entropy effects are significant for the circular-arc cylinder at $M=2.96$ and 4.63, these effects are less than those observed on the circular cone at similar Mach numbers. As a specific example, the entropy decreases the normal force at $M=4.63$ and $\alpha=16$ deg by about 30% for the circular-arc cylinder, but for the circular cone at M = 4.50 and $\alpha=16$ deg (Fig. 7) the normal force is decreased by about 60%.

Surface-pressure results for this circular cross-section body at $M=1.60$ and $\alpha=20$ deg are presented in Fig. 10 for several body stations. The character of the pressure distribution for the most forward body station ($X/L=0.075$) is very similar to that for the circular cone at $M=1.70$ and $\alpha=21$ deg. No separated flow is indicated at this body station. The longitudinal geometry gradients produce an expanding flowfield as evidenced by both the experimental and

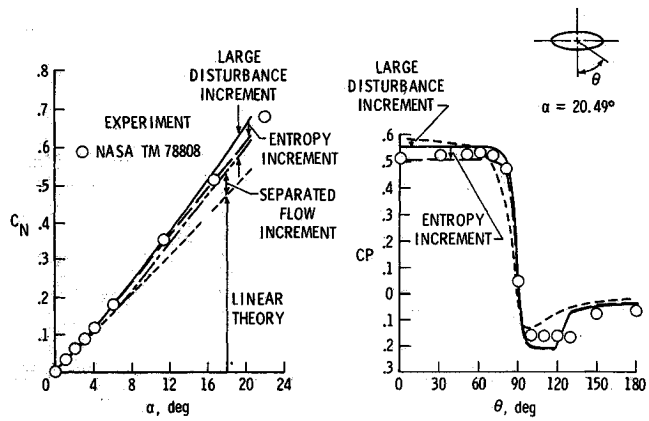

Fig. 6 Normal force and pressure coefficient comparisons for the 3:1 elliptic cone at $M_\infty=2.50$.

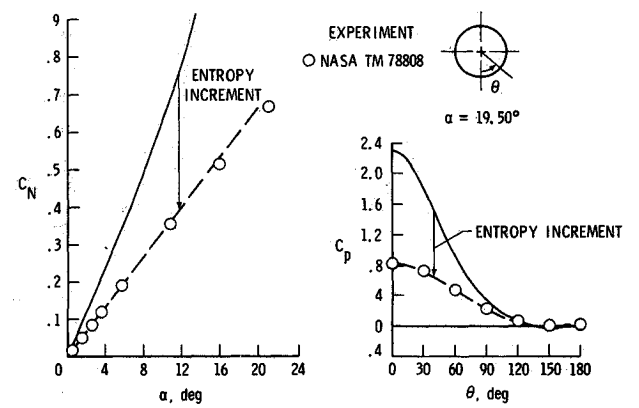

Fig. 7 Normal force and pressure coefficient comparisons for the 20 deg circular cone at $M_\infty=4.50$.

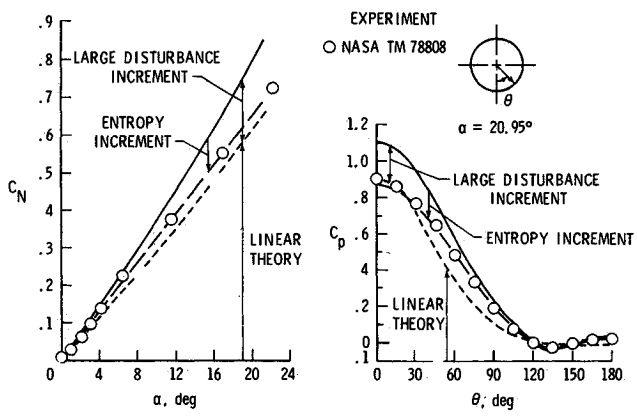

Fig. 5 Normal force and pressure coefficient comparisons for the 20 deg circular cone at $M_\infty=2.50$.

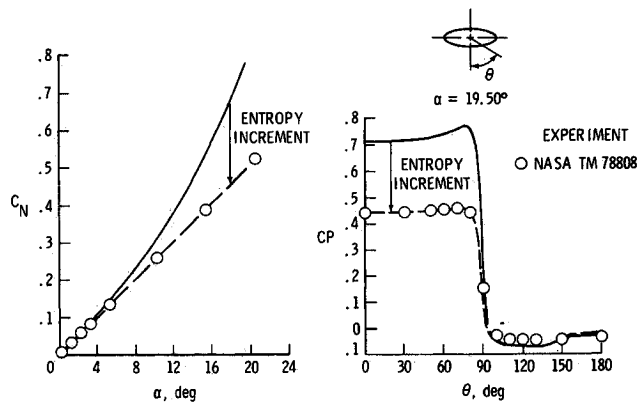

Fig. 8 Normal force and pressure coefficient comparisons for the 3:1 elliptic cone at $M_\infty=4.50$.

theoretical pressure data at $X/L=0.425$ Note that the attached-flow compression pressures have decreased significantly and that flow separation is indicated on the leeward surface The flow separation becomes more pronounced on the cylindrical portion of the body The extent of the separated-flow region can be verified by observing the oil-flow photographs in Ref 11. The large-disturbance increment is also influenced by the longitudinal geometry gradients; in general, the large-disturbance increment is somewhat larger in the areas where the longitudinal geometry gradients are larger As was noted for the normal-force results at $M=1.60$ (Fig. 9), entropy increments in pressure are not significant in regions of attached flow

Surface-pressure results for the same body stations on the circular-arc cylinder body at $M=2\ 96$ and $\alpha=20$ deg are shown in Fig 11 The general behavior of the three-dimensional flowfield is similar to the $M=1\ 60$ case shown in Fig 10, i e , the flowfield continually expands with axial distance from the nose. Leeside flow separation is indicated from the shoulder region of the body aft along the cylinder. The theoretical data follow similar trends, but the levels of the theory with respect to the experiment are quite different from those which were seen at $M=1\ 60$ Both the full potential method and the linear-theory method overestimate compression pressures near the lower-surface centerline for the first two stations, though the general trend of the linear theory is to underestimate compression pressures The overestimation of the linear-theory lower surface pressures near the centerline yielded a more accurate linear-theory estimate for normal force at $M=2\ 96$ compared with the $M=1.60$ case (Fig 9); however, the pressures are actually less accurate at the higher Mach number The entropy is substantially influenced by the longitudinal geometry gradients, as demonstrated by the decreasing magnitude of the entropy increment with increasing axial distance from the nose. Again, it is observed that the entropy increment is primarily confined to the lower surface

The pressure data at $M=4\ 63$ and $\alpha=16$ deg are shown in Fig 12 The data are displayed circumferentially for three body stations and also axially along the lower-surface centerline The centerline data are used to emphasize the magnitude and extent of the entropy increment and the accuracy of the approximate entropy correction. The entropy increment clearly diminishes as the flowfield expands Of course, the same effect of entropy is seen circumferentially at $X/L=0\ 075$, where the entropy effect decreases from the lower-surface centerline The leeside flow appears to be largely separated, although the integrated effect of flow separation does not seem to significantly influence the normal force (Fig 9)

The results for an elliptic body with an Adams' minimum drag area distribution may now be presented and compared with previously discussed results for the 3:1 elliptic cross section cone The complete set of force[13] and surface pressure data[14] are limited to $M=2.50$; therefore, the analysis will be conducted for this Mach number The normal force data at $M=2.50$ are shown in Fig 13. Note that the separated flow increment and the large-disturbance increment are of approximately the same magnitude, but both of these increments are greater in this case than was seen for the elliptic cross-section cone at $M=2.50$ (Fig 6) The entropy effect becomes apparent at $\alpha\approx15$ deg and the magnitude of the increment remains rather small relative to the large disturbance increment. The 3:1 elliptic cross-section cone (Fig 6) showed a similar entropy effect at $M=2\ 50$

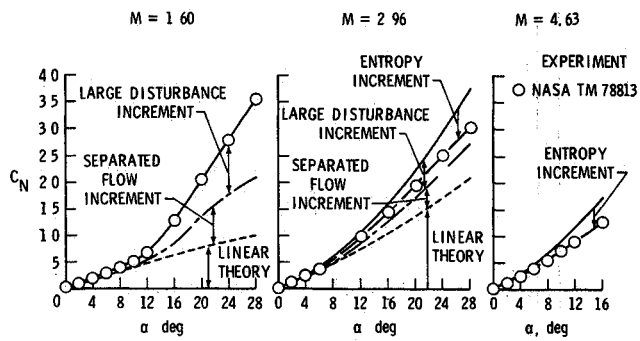

Fig. 9 Normal force coefficient comparisons for the circular-arc cylinder at $M_\infty=1\ 60, 2\ 96$, and 4 63

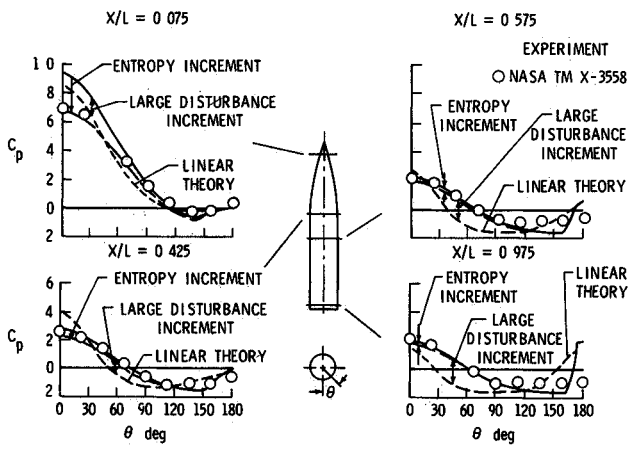

Fig 11 Pressure coefficient comparisons for the circular arc cylinder at $M_\infty=2\ 96$ and $\alpha=20$ deg

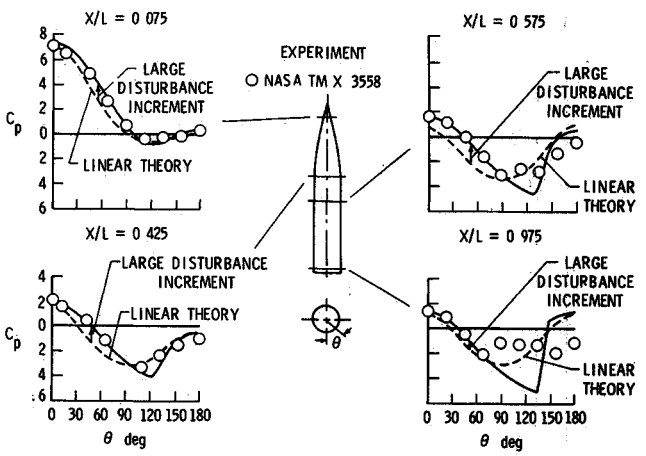

Fig 10 Pressure coefficient comparisons for the circular-arc cylinder at $M_\infty=1.60$ and $\alpha=20$ deg

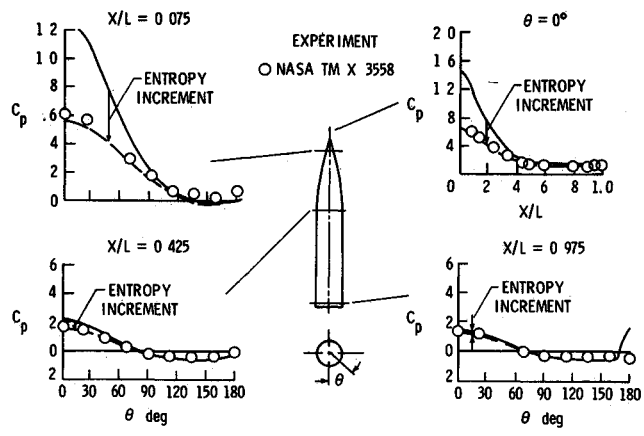

Fig 12 Pressure coefficient comparisons for the circular arc cylinder at $M_\infty=4\ 63$ and $\alpha=16$ deg

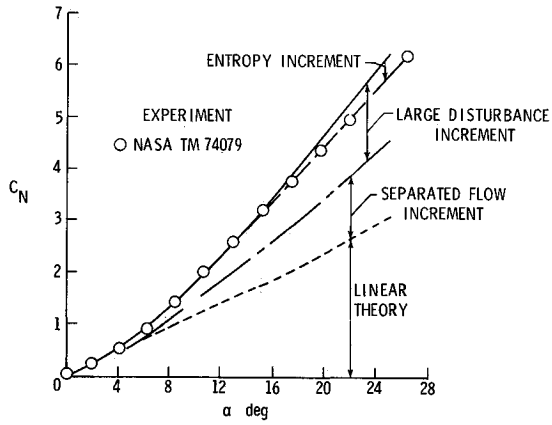

Fig 13 Normal force coefficient comparison for the Adams minimum drag body of 3:1 elliptic cross section at $M_\infty = 2\ 50$

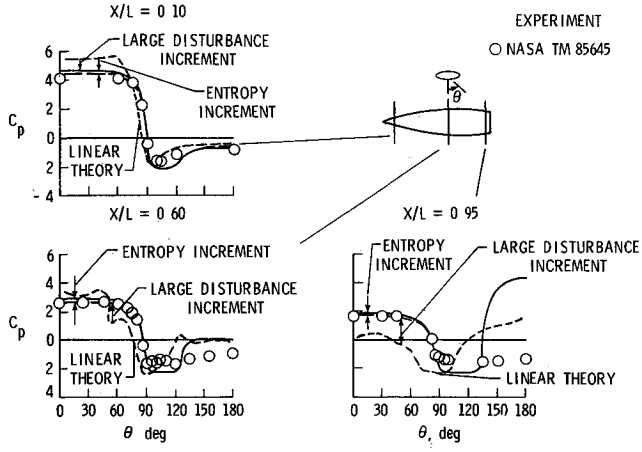

Fig 14 Pressure coefficient comparison for the Adams minimum drag body of 3:1 elliptic cross section at $M_\infty = 2\ 50$ and $\alpha = 20$

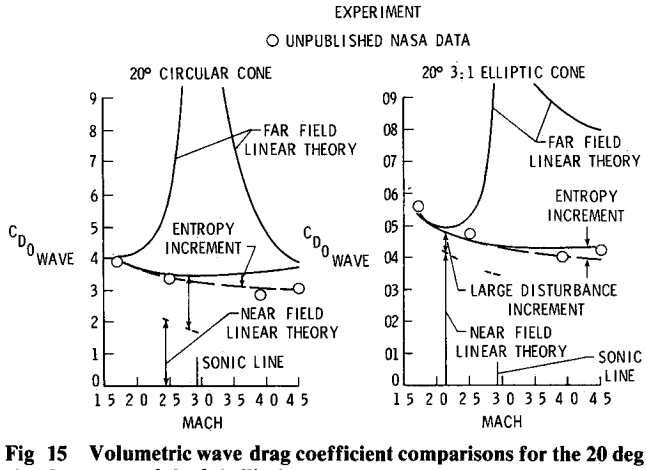

Fig 15 Volumetric wave drag coefficient comparisons for the 20 deg circular cone and the 3:1 elliptic cone

Pressure data for three body stations at $M = 2\ 50$ and $\alpha = 20$ deg are shown in Figure 14 The longitudinal geometry gradients decrease the magnitude of the lower surface compression pressures with axial distance The relatively constant level of lower surface pressures in the spanwise direction indicates a relatively flat lower surface contour Separated leeside flow is indicated along the entire length of the body It is difficult to draw conclusions about the large disturbance increment due to the erratic nature of the linear theory solution, but it is clear from the figure that the full potential solution is much more accurate than the linear theory solution in the attached flow region The rather small changes in the pressure coefficient due to the entropy correction correlate with the small effect on the normal force seen in Fig 13

Axial Force Analysis

Thus far the emphasis has been placed on high angle of attack results where the nonlinear effects on the normal force and pressure coefficient are large; however, at low angle of attack the nonlinear attached flow effects can be significant for axial force In order to show the magnitude of the nonlinear, attached flow effects at low angle of attack, the zero angle of attack inviscid axial force (volumetric wave drag) for the uncambered circular and elliptic cones is examined across the Mach number range in Fig 15

Linear theory wave drag estimates determined by two different types of linear theory methods are shown in Fig 15 The integrated linear theory wave-drag estimate[5,6] (identified as the near field linear theory on the figure) has been used for all linear theory calculations to this point Also included on the figure is the far field wave drag estimate[15] which couples the supersonic area rule with slender body theory The near field solution fails when the freestream Mach cone falls inside the body, as mentioned previously However, this type of linear theory wave drag calculation does not show large errors when the body lies just inside the Mach cone—the case for the far-field method The nonlinear full potential method produces a much more accurate drag estimate and is not affected by Mach cone limitations The entropy increment reduces the wave drag at high Mach number even for $\alpha = 0$ deg This effect is larger and becomes apparent at a lower Mach number for the circular cone than for the thinner 3:1 elliptic cross section cone

Conclusions

The supersonic flow about two dimensional and three dimensional bodies was analyzed to identify the nonlinear aerodynamic effects on bodies of circular and elliptic cross section These effects were identified as a separated flow nonlinear increment and an attached flow nonlinear in crement which was further divided into a large-disturbance effect and an entropy effect Attached flow boundaries were developed to illustrate the flow regimes where the nonlinear effects are significant and the use of these boundaries for angle of attack and for three dimensional geometries was indicated

The investigation focused on comparisons of experimental and theoretical pressure coefficient and normal force coefficient A full potential method, NCOREL, which in cludes an approximate entropy correction, was shown to provide accurate attached flow pressure and normal force estimates from Mach 1 6 through Mach 4 6 A procedure was developed for the normal force comparisons that allowed the separated flow increment to be determined without explicitly calculating the local effects of flow separation

With increasing Mach number, the results showed these trends: 1) the magnitude of the separated flow increment decreased; 2) the magnitude of the large disturbance in crement decreased or remained nearly constant; and 3) the magnitude of the entropy increment increased Both the separated flow and large disturbance increments increased the normal force, but the entropy increment decreased the normal force Entropy did not affect appreciably the at tached flow result below approximately Mach 2 Also the magnitude of the nonlinear normal force increments was small at low angle of attack but increased significantly at high angle of attack

The effect of cross section shape was shown by considering a circular and a 3:1 elliptic cross section cone of equivalent planform The cross section shape significantly influenced the magnitude and distribution of the pressure coefficient

nonlinear increments as well as the magnitude of the normal force nonlinear increments In particular, the thinner elliptic cone produced separated leeside flow and the circular cone showed a larger effect due to the large disturbance increment and the entropy increment Analysis of three dimensional bodies indicated that longitudinal geometry gradients in creased the contribution of the large disturbance and separated flow increments, but decreased the entropy in crement The pressure data showed that the entropy increment was strongest at the nose and decreased in magnitude with axial distance from the nose Also, the effect of separated flow tended to be small near the nose, but of increasing magnitude with axial distance from the nose The large disturbance and entropy increments were shown to significantly affect the volumetric wave drag calculation of the conical geometries The nonlinear full-potential method, NCOREL, provided much more accurate wave-drag estimates than the linear-theory methods and was not restricted by the freestream Mach cone limitations which limit the range of linear-theory methods.

References

[1]Smith, C A. and Nielsen J N Prediction of Aerodynamic Characteristics of Cruciform Missiles to High Angles of Attack Utilizing a Distributed Vortex Wake' Nielsen Engineering and Research, Inc., Mountain View, Calif TR 208, Jan 1980.

[2]Dillenius, M F E and Nielsen J. N. Computer Programs for Calculating Pressure Distributions Including Vortex Effects on Supersonic Monoplane or Cruciform Wing Body Tail Combinations with Round or Elliptical Bodies NASA CR 3122 April 1979

[3]Allen J M and Pittman J L Analysis of Surface Pressure Distributions on Two Elliptic Missile Configurations AIAA Paper 83-1841, July 1983

[4]Sims, J L ' Tables for Supersonic Flow Around Right Circular Cone at Zero Angle of Attack NASA SP 3004 1964

[5]Woodward, F A , An Improved Method for the Aerodynamic Analysis of Wing Body Tail Configurations in Subsonic and Supersonic Flow Part I—Theory and Application, NASA CR 2228 May 1973

[6]Woodward, F A An Improved Method of the Aerodynamic Analysis of Wing Body Tail Configurations in Subsonic and Supersonic Flow Part II—Computer Program Description ' NASA CR 2228 May 1973

[7]Siclari, M J The NCOREL Computer Program for 3D Nonlinear Supersonic Potential Flow Computations,' NASA CR 3694 Aug 1983

[8]Mason W H. and Rosen B S 'The COREL and W12SC3 Computer Programs for Supersonic Wing Design and Analysis, NASA CR 3676, 1983

[9]Siclari M. J and Visich M , 'Shock Fitting in Conical Supersonic Full Potential Flows with Entropy Effects ' AIAA Paper 84-0261, Jan 1984

[10]Townsend J C Collins, I K , Howell, D T , and Hayes C , 'Surface Pressure Data on a Series of Conical Forebodies at Mach Numbers from 1 70 to 4 50 and Combined Angles of Attack and Sideslip NASA TM 78808 March 1979

[11]Landrum, E. J and Babb C D Wind Tunnel Force and Flow Visualization Data at Mach Numbers from 1 6 to 4 63 for a Series of Bodies of Revolution at Angles of Attack from −4 to 60° ' NASA TM 78813 March 1979

[12]Landrum, E J , Wind-Tunnel Pressure Data at Mach Numbers from 1.6 to 4 63 for a Series of Bodies of Revolution at Angles of Attack from −4° and 60° " NASA TM X 3558 Oct 1977

[13]Graves, E B , ' Aerodynamic Characteristics of a Monoplanar Missile Concept with Bodies of Circular and Elliptical Cross Section ' NASA TM 74079, Dec. 1977

[14]Allen, J. M Hernandez, G and Lamb M , Body Surface Pressure Data on Two Monoplane Wing Missile Configurations with Elliptical Cross Sections at Mach 2 50 NASA TM 85645 Sept 1983

[15]Harris, R V., ' An Analysis and Correlation of Aircraft Wave Drag NASA TM X 947 March 1964.